Progress In Electromagnetics Research C, Vol. 62, 43–50, 2016

Analysis and Design of Rectangular Uniaxial and Biaxial Anisotropic Dielectric Resonator Antennas

Saeed Fakhte* **and Homayoon Oraizi**

Abstract—An anisotropic dielectric resonator antenna (ADRA) with uniaxial and biaxial permittivity tensors is characterized by using the dielectric waveguide model. An approximate formula for the Q factor of ADRA is derived. Then, it is shown that by certain conditions a wideband ADRA can be designed. Samples of simulation results are shown to demonstrate the capabilities of the proposed anisotropic technique for enhancing the bandwidth of ADRA. The proposed antenna is simulated by two full wave packages, Ansoft HFSS and CST Microwave Studio, and a good agreement is observed among the results.

1. INTRODUCTION

Dielectric resonator antennas (DRAs) have received much attention due to several attractive characteristics, such as light weight, low profile and high radiation efficiency [1–7]. Even though DRAs were originally devised for millimeter-wave applications, they are also extensively studied at microwave frequency. Resonant frequencies, Q factors, field distributions and radiation properties of resonant modes of the isotropic DRA have been extensively analysed by various methods. Basic characteristics of DRA resonant modes are treated in [1, 2]. The much of the literature investigates isotropic cases. Crystals (such as calcite and sapphire) are examples of natural anisotropic materials. The single crystal rutile has a dielectric anisotropy at GHz frequencies, but its high cost prevents practical use. Recently, the investigation and characterization of anisotropic materials have been intensively carried out, owing to the recent advances in material science and technology. They have also been applied in microwave engineering and electromagnetic scattering [8]. Dielectric resonators (DRs) made of crystal materials, such as sapphire, have received substantial attention due to their very low loss nature for fabricating high-stability and low-noise microwave oscillators [9–11]. In addition to the extensively used sapphire material, other materials for building very low loss DRs are also reported [12]. Approximate and rigorous solutions have been used to obtain the resonant frequency and field distribution of a cylindrical anisotropic DR [13–15].

The literature on the analysis of anisotropic DRA is limited compared to that of isotropic DRA, and almost all the preceding DRA structures handle uniform or multilayer isotropic volumes (except the ferrite DRAs [16]). The development of ferrite resonator antenna was reported by Petosa et al. [16]. The approximate analysis of uniaxial-anisotropic DRA has been performed in [17] using the PMC cavity model.

In this paper, the dielectric waveguide model is used to estimate the resonant frequency and radiation Q factor for a rectangular ADRA. Note that the dielectric waveguide model is more accurate than PMC cavity model. In fact, PMC cavity model is only applicable for the DR with a very high dielectric constant. Several samples of uniaxial ADRA are simulated, and their impedance bandwidths

Received 28 December 2015, Accepted 5 February 2016, Scheduled 11 February 2016

* Corresponding author: Saeed Fakhte (saeedfakhte@elec.iust.ac.ir).

The authors are with the Department of Electrical Engineering and Center of Excellence in Railway Transportation, Iran University of Science and Technology, Tehran, Iran.

are discussed. It is observed that a wideband design can be achieved by decreasing only one element of permittivity tensor.

2. THEORY

Consider a y-direction dielectric waveguide of a rectangular cross section $a \times b$, filled uniformly by an anisotropic medium with

$$\bar{\bar{\varepsilon}} = \begin{pmatrix} \varepsilon_x & 0 & 0 \\ 0 & \varepsilon_y & 0 \\ 0 & 0 & \varepsilon_z \end{pmatrix}, \quad \bar{\bar{\mu}} = \begin{pmatrix} \mu_x & 0 & 0 \\ 0 & \mu_y & 0 \\ 0 & 0 & \mu_z \end{pmatrix} \tag{1}$$

The field distribution in the dielectric waveguide satisfies the source-free curl Maxwell equations

$$\begin{aligned} \nabla \times \bar{E} &= -j\omega \bar{\bar{\mu}} \bar{H} \\ \nabla \times \bar{H} &= j\omega \bar{\bar{\varepsilon}} \bar{E} \end{aligned} \tag{2}$$

Assuming $\bar{E}(x, y, z) = \bar{E}(x, z)e^{-\gamma y}$ and $\bar{H}(x, y, z) = \bar{H}(x, z)e^{-\gamma y}$, in the case of TE^y modes, the following equations are derived

$$E_x = \frac{j\omega\mu_0\mu_z}{k_0^2\mu_z\varepsilon_x + \gamma^2} \frac{\partial H_y}{\partial z} \tag{3a}$$

$$E_z = \frac{-j\omega\mu_0\mu_x}{k_0^2\mu_x\varepsilon_z + \gamma^2} \frac{\partial H_y}{\partial x} \tag{3b}$$

$$H_x = \frac{1}{\gamma^2 + k_0^2\mu_x\varepsilon_z} \frac{\partial^2 H_y}{\partial x \partial y} \tag{3c}$$

$$H_z = \frac{1}{\gamma^2 + k_0^2\mu_z\varepsilon_x} \frac{\partial^2 H_y}{\partial y \partial z} \tag{3d}$$

Eliminating the electric field $\bar{E}$ from Eq. (2) leads to the following vector wave equation satisfied by the magnetic field $\bar{H}$:

$$\nabla \times \bar{\bar{\varepsilon}}^{-1}(\nabla \times \bar{H}) = k_0^2 \bar{\bar{\mu}} \bar{H} \tag{4}$$

Substituting Eq. (3) into Eq. (4) leads to

$$\frac{k_0^2\mu_x}{\gamma^2 + k_0^2\mu_x\varepsilon_z} \frac{\partial^2 H_y}{\partial x^2} + \frac{k_0^2\mu_z}{\gamma^2 + k_0^2\mu_z\varepsilon_x} + k_0^2\mu_y H_y = 0 \tag{5}$$

In essence, the method of separation of variables seeks a solution of Eq. (5) of the form

$$H_y = X(x)Z(z)e^{-\gamma y} \tag{6}$$

The losses in the waveguide are neglected. So, the waveguide propagation constant γ is pure-imaginary:

$$\gamma = jk_y \tag{7}$$

By enforcing PMC boundary conditions for the waveguide structure of Fig. 1 which requires the tangential components of magnetic field to vanish on the walls of the waveguide, the following solution of Eq. (7) is obtained

$$H_y(x, y, z) = H_0 \sin\left(k_x\left(x + \frac{a}{2}\right)\right) \sin\left(k_z\left(z + \frac{d}{2}\right)\right) e^{-jk_y y} \tag{8}$$

The dispersion relation for the waveguide is determined by substituting Eq. (8) in Eq. (5):

$$\begin{aligned} &\frac{k_x^2\mu_x}{k_0^2\mu_x\varepsilon_z - k_y^2} + \frac{k_z^2\mu_z}{k_0^2\mu_z\varepsilon_x - k_y^2} = \mu_y \\ &k_x = \frac{m\pi}{a}, \quad k_z = \frac{l\pi}{d} \end{aligned} \tag{9}$$

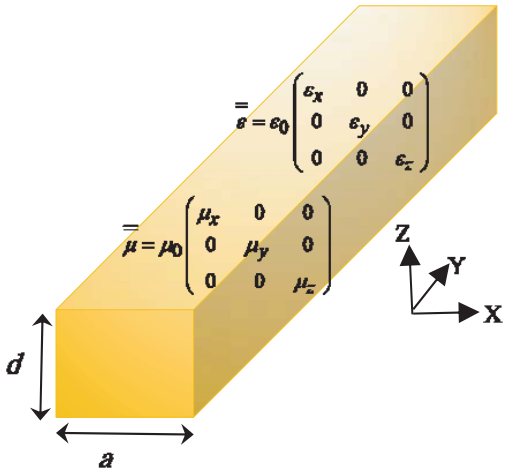

Figure 1. 3D view of the anisotropic dielectric waveguide.

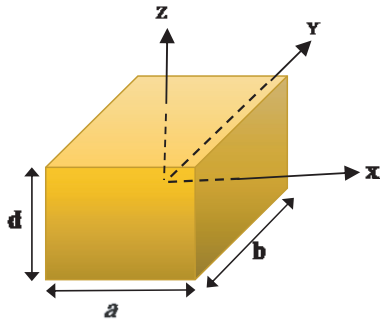

Figure 2. Truncated anisotropic dielectric waveguide.

Inserting Eq. (8) into Eq. (3) leads to the field expressions for the TE^y mode in the anisotropic dielectric waveguide

$$E_x = \frac{-j\omega\mu_0\mu_z H_0 k_z}{k_0^2\mu_z\varepsilon_x - k_y^2} \times \sin\left(k_x\left(x+\frac{a}{2}\right)\right)\cos\left(k_z\left(z+\frac{d}{2}\right)\right)e^{-jk_y y} \tag{10a}$$

$$E_y = 0 \tag{10b}$$

$$E_z = \frac{j\omega\mu_0\mu_x H_0 k_x}{k_0^2\mu_x\varepsilon_z - k_y^2} \times \cos\left(k_x\left(x+\frac{a}{2}\right)\right)\sin\left(k_z\left(z+\frac{d}{2}\right)\right)e^{-jk_y y} \tag{10c}$$

$$H_x = \frac{jH_0 k_x k_y}{k_0^2\mu_x\varepsilon_z - k_y^2} \times \cos\left(k_x\left(x+\frac{a}{2}\right)\right)\sin\left(k_z\left(z+\frac{d}{2}\right)\right)e^{-jk_y y} \tag{10d}$$

$$H_z = \frac{jH_0 k_z k_y}{k_0^2\mu_z\varepsilon_x - k_y^2} \times \sin\left(k_x\left(x+\frac{a}{2}\right)\right)\cos\left(k_z\left(z+\frac{d}{2}\right)\right)e^{-jk_y y} \tag{10e}$$

To model the dielectric resonator antenna, the waveguide is truncated along the y-direction at $y = \pm b/2$, as shown in Fig. 2, and replaced by two air-filled hollow waveguides, which operate below cutoff because they are filled with low dielectric constant material. Therefore, the modes in these air-filled PMC waveguides are evanescent, wherein the fields decay exponentially in the y direction away from each end of the resonator.

In the air region, for $|y| > b/2$, the waveguide propagation constant γ is pure-real:

$$\gamma = \alpha \tag{11}$$

Then the y-directed magnetic field, H_y, for the TE^y mode can be written for $|y| > b/2$ as

$$H_y(x,y,z) = H_1 \sin\left(k_x\left(x+\frac{a}{2}\right)\right)\sin\left(k_z\left(z+\frac{d}{2}\right)\right)e^{-\alpha y} \tag{12}$$

And for $|y| < b/2$ as

$$H_y(x,y,z) = H_0 \sin\left(k_x\left(x+\frac{a}{2}\right)\right)\cos(k_y y)\sin\left(k_z\left(z+\frac{d}{2}\right)\right) \tag{13}$$

Matching the tangential fields at $y = b/2$ (or $y = -b/2$) leads to the following transcendental

equation for the wavenumber k_y of TE^y_{mnl} mode

$$k_y b = 2\tan^{-1}\left(\frac{\mu_z\sqrt{k_x^2+k_z^2-k_0^2}}{k_y}\right) \tag{14a}$$

$$k_x = \frac{m\pi}{a}, \quad k_z = \frac{l\pi}{d} \tag{14b}$$

$$\frac{k_x^2\mu_x}{k_0^2\mu_x\varepsilon_z - k_y^2} + \frac{k_z^2\mu_z}{k_0^2\mu_z\varepsilon_x - k_y^2} = \mu_y \tag{14c}$$

Consequently, the fields within DRA are

$$E_x = -\frac{j\omega\mu_0\mu_z k_z H_0}{k_0^2\mu_z\varepsilon_x - k_y^2} \times \sin\left(k_x\left(x+\frac{a}{2}\right)\right)\cos(k_y y)\cos\left(k_z\left(z+\frac{d}{2}\right)\right) \tag{15a}$$

$$E_y = 0 \tag{15b}$$

$$E_z = \frac{j\omega\mu_0\mu_x k_x H_0}{k_0^2\mu_x\varepsilon_z - k_y^2} \times \cos\left(k_x\left(x+\frac{a}{2}\right)\right)\cos(k_y y)\sin\left(k_z\left(z+\frac{d}{2}\right)\right) \tag{15c}$$

$$H_x = \frac{H_0 k_y k_x}{k_0^2\mu_x\varepsilon_z - k_y^2} \times \cos\left(k_x\left(x+\frac{a}{2}\right)\right)\sin(k_y y)\sin\left(k_z\left(z+\frac{d}{2}\right)\right) \tag{15d}$$

$$H_z = \frac{H_0 k_y k_z}{k_0^2\mu_z\varepsilon_x - k_y^2} \times \sin\left(k_x\left(x+\frac{a}{2}\right)\right)\sin(k_y y)\cos\left(k_z\left(z+\frac{d}{2}\right)\right) \tag{15e}$$

For a rectangular DRA with dimensions $a, d > b$, the lowest order mode will be TE^y_{111}. The radiation Q factor of the anisotropic DRA can be found by determining the total stored energy and the power radiated by the DRA. The radiation Q factor of ADRA for the TE^y_{111} mode is determined by the method reported in [18].

$$Q_{rad} = \frac{\pi^4(1+\mathrm{sinc}(k_y b))}{64k_0^5 \mathrm{abd}\,\mathrm{sinc}^2(k_y b/2)} \times \frac{\varepsilon_x\dfrac{k_z^2}{(k_0^2\varepsilon_x - k_y^2)^2} + \varepsilon_z\dfrac{k_x^2}{(k_0^2\varepsilon_z - k_y^2)^2}}{\left[\dfrac{k_z d(\varepsilon_x - 1)}{k_0^2\varepsilon_x - k_y^2} + \dfrac{k_x a(\varepsilon_z - 1)}{k_0^2\varepsilon_z - k_y^2}\right]^2} \tag{16}$$

To investigate the effect of anisotropy on the DRA performance, four samples of DRA with different permittivity tensors but the same aspect ratios are studied (Table 1). For case A, an isotropic DRA with TE^y_{111} mode at 3.7 GHz is designed. Observe in Table 1 that by lowering the ε_z from 20 in case A to 5 in case D, Q factor of the antenna is decreased, and consequently the impedance bandwidth is increased. This is in agreement with the closed form expression for Q factor of ADRA in Equation (16).

Table 1. Theoretical radiation Q factor and bandwidth of anisotropic DRA. $f_0 = 3.7$ GHz, $b/a = 0.6$, $d/a = 0.8$, $\varepsilon_x = 20$.

CASE	a (mm)	f (Sim.)	h_p	ε_z	Q_{rad}	BWT (%)	BWS (%)
A	17.7	3.79	6.5	20	19.8	3.6	3.4
B	18.65	3.74	6.2	15	16.4	4.3	3.5
C	20.25	3.59	5.9	10	12.1	5.8	5
D	27.43	3.16	6	5	6.8	10.5	7.1

3. SIMULATION

The DRA samples are simulated using HFSS (Fig. 3). The optimized values of the probe heights are listed in Table 1. The simulated results of reflection coefficient are shown in Fig. 4. It can be seen

that the resonant frequency of case D is noticeably shifted down from the design resonant frequency 3.7 GHz, which is expected because of the very low value of $\varepsilon_z = 5$. The simulated resonant frequencies of the other cases are approximately equal to the design resonant frequency. These four cases are also simulated by CST software, and a good agreement is observed between the results of HFSS and CST, as shown in Fig. 4(b).

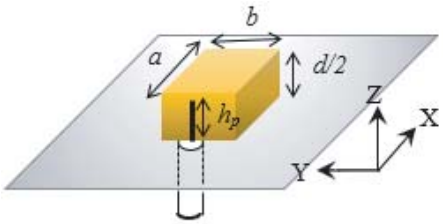

Figure 3. A probe-fed anisotropic DRA.

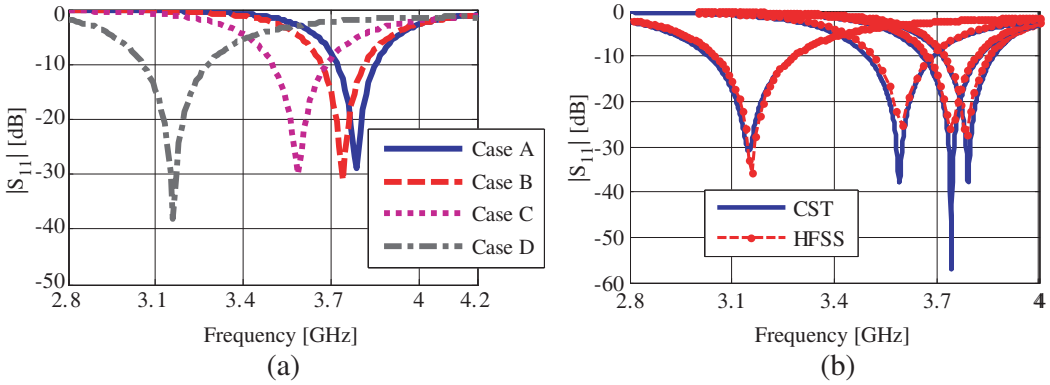

Figure 4. Simulated reflection coefficient of the Anisotropic DRAs. (a) DRA cases of A, B, C and D; (b) Comparison between the results of CST and HFSS.

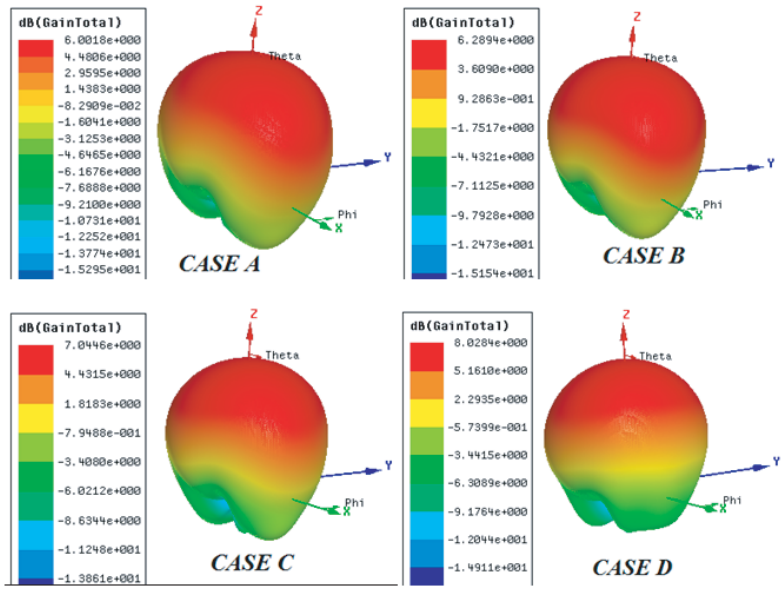

Figure 5. Simulated 3D radiation patterns (gains) of the Anisotropic DRA for different cases at their resonant frequencies (see Table 1).

The simulated 10 dB-impedance bandwidth for cases A, B, C, and D are about 3.4%, 3.5%, 5% and 7.1% (see Table 1). Compared to the achieved 3.4% bandwidth of the isotropic DRA (Case A), the use of uniaxial anisotropic dielectric in the DRA cube can offer an increase of the impedance bandwidth. An increase in simulated impedance bandwidths is observed due to the lowering of Q-factor. In fact, by decreasing the value of ε_z, the value of Q-factor in Eq. (16) is decreased, and consequently the impedance bandwidth is increased. Observe in Table 1 that the simulated impedance bandwidths, BWS, are approximately equal to the predicted ones using DWM, BWT.

The simulated radiation patterns (gains) of the four antenna samples are shown in Fig. 5. The broadside radiation patterns for all cases are observed. Also, the gain for different cases is above 5 dB. The simulated radiation efficiencies are above the 90% and not included here for brevity. Observe in Fig. 6 that the simulated axial ratio for all cases is above 40 dB. So, these ADRAs are linearly polarized antennas.

The next higher order TE^{y}_{311} mode is excitable in these anisotropic DRAs. The predicted and simulated resonant frequencies are listed in Table 2. Also, the simulated radiation patterns and gains of these cases are drawn in Fig. 7. A good agreement is observed between the theoretical and simulated results.

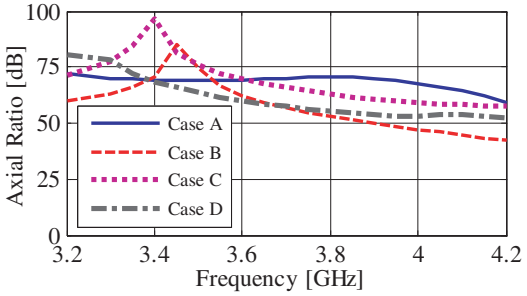

Figure 6. Simulated axial ratio of the Anisotropic DRA for different cases.

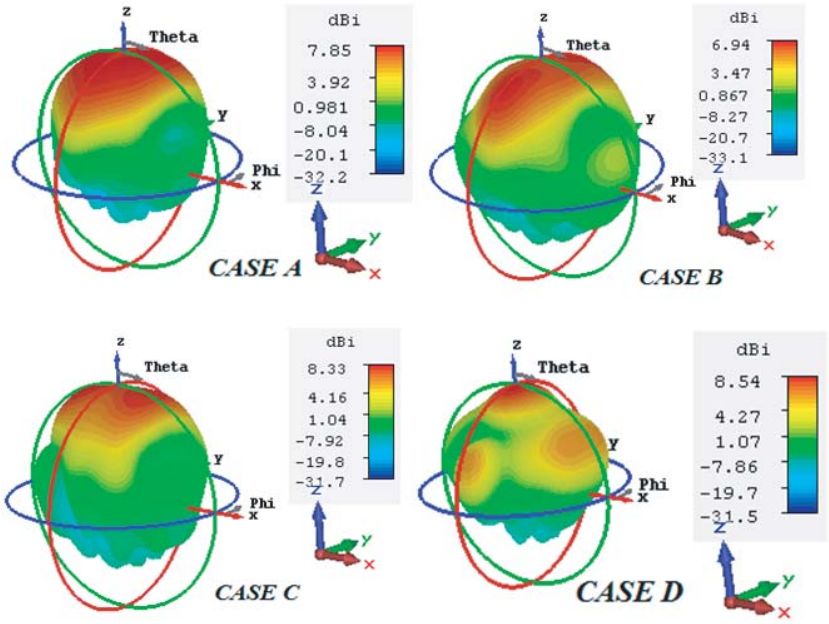

Figure 7. Simulated 3D radiation patterns and gains of the Anisotropic DRA at TE^{y}_{311} mode for different cases at their resonant frequencies (see Table 1). The results are obtained by CST Microwave Studio.

Table 2. Theoretical and simulated resonant frequencies of TE^{y}_{311} mode of anisotropic DRAs.

CASE	f_0 (GHz) Theory	f_0 (GHz) Simulation
A	6.76	6.6
B	7.11	6.7
C	7.64	7.39
D	8.07	7.8

4. CONCLUSION

The uniaxially anisotropic rectangular dielectric resonator antenna (ADRA) is fully investigated in this paper. It has been found that the impedance bandwidth of the ADRA is improved compared to the isotropic DRA. The theoretical investigations on impedance bandwidth of ADRA are carried out. The theoretical results reported here are useful in the design and understanding of ADRA.

REFERENCES

1. Petosa, A., *Dielectric Resonator Antenna Handbook*, Artech House, Norwood, MA, 2007.
2. Luk, K. M. and K. W. Leung, *Dielectric Resonator Antennas*, Research Studies, Baldock, Hertfordshire, U.K., 2003.
3. Petosa, A. and A. Ittipiboon, "Dielectric resonator antennas: A historical review and the current state of the art," *IEEE Antennas and Propagation Magazine*, Vol. 52, No. 5, 91–116, Oct. 2010.
4. Leung, K. W., E. H. Lim, and X. S. Fang, "Dielectric resonator antennas: From the basic to the aesthetic," *Proc. IEEE*, Vol. 100, No. 7, 2181–2193, Jul. 2012.
5. Fakhte, S., H. Oraizi, and M. H. Vadjed-Samiei, "A high gain dielectric resonator loaded patch antenna," *Progress In Electromagnetics Research C*, Vol. 30, 147–158, 2012.
6. Fakhte, S., H. Oraizi, R. Karimian, and R. Fakhte, "A new wideband circularly polarized stair-shaped dielectric resonator antenna," *IEEE Trans. Antennas Propag.*, Vol. 63, No. 4, 1828–1832, Apr. 2015.
7. Fakhte, S., H. Oraizi, and R. Karimian, "A novel low cost circularly polarized rotated stacked dielectric resonator antenna," *IEEE Antennas and Wireless Propag. Lett.*, Vol. 13, 722–725, Apr. 2014.
8. Wong, K. L. and H. T. Chen, "Electromagnetic scattering by a uniaxially anisotropic sphere," *IEE Proceedings H — Microwaves Antennas and Propagation*, Vol. 139, No. 4, 314–318, 1992.
9. Dick, G. J. and J. Saunders, "Measurement and analysis of a microwave oscillator stabilized by a sapphire dielectric ring resonator for ultra low noise," *IEEE Trans. Ultrason. Ferroelect. Freq. Contr.*, Vol. 37, 339–346, Sep. 1990.
10. Tobar, M. E., E. N. Ivanov, R. A. Woode, J. H. Searls, and A. G. Mann, "Low noise 9 GHz sapphire resonator-oscillator with thermoelectric temperature stabilization at 300 Kelvin," *IEEE Microwave Guided Wave Lett.*, Vol. 5, 108–110, Apr. 1995.
11. Giles, A. J., S. K. Jones, D. G. Blair, and M. J. Buckingham, "A very high stability sapphire loaded superconducting cavity osciilator," *Physics B*, Vol. 165, 145–146, 1990.
12. Krupka, J., R. G. Geyer, M. Kuhn, and J. H. Hinken, "Dielectric properties of single crystals of Al_2O_3, $LaAlO_3$, $NdGaO_3$, $SrTiO_3$, and MgO at cryogenic temperatures," *IEEE Trans. Microwave Theory Tech.*, Vol. 42, 1886–1890, Oct. 1994.
13. Tobar, M. E. and A. G. Mann, "Resonant frequencies of higher order modes in cylindrical anisotropic dielectric resonators," *IEEE Trans. Microwave Theory Tech.*, Vol. 39, 2077–2082, Dec. 1991.

14. Krupka, J., "Resonant modes in shielded cylindrical ferrite and single-crystal dielectric resonators," *IEEE Trans. Microwave Theory Tech.*, Vol. 37, 691–697, Apr. 1989.
15. Kobayashi, Y. and T. Senju, "Resonant modes in shielded uniaxial- anisotropic dielectric rod resonators," *IEEE Trans. Microwave Theory Tech.*, Vol. 41, 2198–2205, Dec. 1993.
16. Petosa, A., R. K. Mongia, M. Cuhaci, and J. Wight, "Magnetically tunable ferrite resonator antenna," *Electron. Lett.*, Vol. 30, No. 13, 1021–1022, 1994.
17. Yarga, S., K. Sertel, and J. Volakis, "Multilayer dielectric resonator antenna operating at degenerate band edge modes," *IEEE Antennas and Wireless Propag. Lett.*, Vol. 8, 287–290, 2009.
18. Mongia, R. K. and A. Ittipiboon, "Theoretical and experimental investigations on rectangular dielectric resonator antennas," *IEEE Trans. Antennas Propag.*, Vol. 45, No. 9, 1348–1356, Sep. 1997.